Available online at www.sciencedirect.com
SCIENCE DIRECT®
C. R. Physique 5 (2004) 305–313
COMPTES RENDUS PHYSIQUE

Highly polarized nuclear spin systems and dipolar interactions in NMR/Systèmes de spins nucléaires fortement polarisés et interactions dipolaires en RMN

Mapping hydrophobic molecular regions using dissolved laser-polarized xenon NMR

Lionel Dubois, Patrick Berthault *, J. Gaspard Huber, Hervé Desvaux *

Laboratoire commun de RMN, DSM/DRECAM/service de chimie moléculaire, URA CEA/CNRS 331 Claude Fréjacques, CEA/Saclay, 91191 Gif-sur-Yvette, France

Available online 9 April 2004

Presented by Guy Laval

Abstract

Molecular hydrophobic cavities can be mapped thanks to the detection of magnetization transfer from laser polarized xenon to nearby protons. This so called SPINOE approach is described. The study of the spin dynamics during this experiment and its consequences on the practical implementation are detailed. We show that thanks to the knowledge of the physical properties of the system, it becomes possible to choose the best experimental conditions in order to be able to assign magnetization transfer through two dimensional NMR methods. As an illustration, the first 2D SPIROE-TOCSY experiment is reported. ***To cite this article: L. Dubois et al., C. R. Physique 5 (2004).***

Résumé

Cartographie des régions moléculaires hydrophobes par RMN du xénon polarisé par laser dissous. Les régions moléculaires hydrophobes peuvent être localisées par l'approche appelée SPINOE qui consiste en la détection des transferts d'aimantation du xénon polarisé par laser dissous vers les protons proches du soluté. Nous rapportons l'étude de la dynamique présente lors de cette expérience et discutons les conséquences sur son implémentation. Nous montrons que la connaissance des propriétés physico-chimiques du système permet de choisir les meilleures conditions expérimentales afin d'être capable d'identifier les transferts d'aimantation via des expériences de RMN à deux dimensions. Nous illustrons ce résultat par le premier spectre de SPIROE-TOCSY. ***Pour citer cet article : L. Dubois et al., C. R. Physique 5 (2004).***

Keywords: NMR; Laser polarized xenon; SPINOE; Protein hydrophobic cavity

Mots-clés : RMN ; Xénon polarisé par laser ; SPINOE ; Cavité hydrophobe de protéines

1. Introduction

The recent availability of very high-field NMR spectrometers and of cryoprobeheads cannot mask the poor sensitivity of this spectroscopy inherent to the low nuclear polarization. Indeed at Boltzmann equilibrium, the nuclear polarization of proton spins is only 5×10^{-5} at 14 Tesla and room temperature. Several solutions to increase the NMR signal by using magnetization transfer from more polarized systems such as electron spins or para-hydrogen are described in this Issue. Here the solution based on optical pumping is explored. It is indeed known since the early 1950s that light polarization can be transferred leading to high

* Corresponding authors.
E-mail addresses: pberthault@Cea.fr (P. Berthault), hdesvaux@Cea.fr (H. Desvaux).

1631-0705/$ – see front matter
doi:10.1016/j.crhy.2004.02.003

electronic polarization [1], and since 1960 that this method can be used to enhance the NMR signal [2]. In the spin-exchange experiment, the transfer of the light angular momentum to electronic spins of an alkali metal, and then to the nuclear spins of the noble gas through collisions [3] is performed. This process is particularly efficient for noble gases of spin $\frac{1}{2}$ (^{3}He and ^{129}Xe) which relax slowly. The choice between these two gases is usually made according to their applications. In MRI experiments, helium has been shown to be an excellent candidate for the probing of lung alveoli [4]. Xenon is more interesting for the study of vessels, as its solubility in blood is far from negligible [5]. From the spectroscopist's point of view, xenon has many advantages over helium. Firstly, its solubility in various liquids is higher than that of helium. Secondly, the high polarizability of its electronic cloud gives this atom a pronounced hydrophobic character, and leads its chemical shift to span a range of several hundred ppm. Thus, xenon NMR is very rich in information and has been used for the study of high specific surface materials, including zeolites and mesoporous materials [6–9]. Finally, laser-polarized xenon allows the detection and characterization of protein pockets [10,11] thanks to its hydrophobic properties. The present paper gives an overview of the characterization of molecular pockets using laser-polarized xenon. It mainly emphasizes the recent experiments designed to observe selective magnetization transfer. It also shows that, thanks to the fine characterization of the spin dynamics, it becomes possible to correctly tune the experimental parameters in order to control the magnetization transfer and then to use multidimensional NMR techniques for safe assignment of the protons close to the xenon atom. The first experimental illustration is reported.

2. Detection of protein hydrophobic cavities

The catalytic site of many proteins is constituted of an hydrophobic region bordered by apolar residues. A recurrent debate exists about the presence or the absence of disordered water molecules buried in these cavities, and about their role during the ligand binding [12,13]. Indeed the most important host-guest interaction in aqueous solutions is based on attraction between lipophilic regions of the two molecules. This classical hydrophobic effect is enhanced by a release of water molecules and a corresponding gain in entropy. Principally, two physical methods enable detection at the atomic resolution of these hydrophobic regions: X-Ray crystallography and NMR spectroscopy.

- X-ray crystallographers either indirectly detect these cavities by the defect of electronic density, or use noble gases such as krypton or xenon under medium to high pressure [14–16]. The protocol is the following: the protein crystal is pressurized by the noble gas which diffuses in it toward these cavities. By using the Fourier difference of diffraction patterns the hydrophobic regions filled by the noble gas atoms are identified. It appears experimentally that the occupation factors of the cavities are strongly correlated to the fitting of the cavity size to the atomic volume.
- The first NMR approaches for the study of these hydrophobic protein pockets used through-space magnetization transfer from small apolar molecules to protons of the protein [17]. The inefficiency of the intermolecular dipolar cross-relaxation is compensated by the high concentration employed for these apolar molecules, obtained either by working at the limit of solubility (for compounds such as benzene or cyclohexane), or under high pressure (for methane, ethane, ...). It remains that the risk of distortion of the protein induced by these high pressures is far from negligible.

The perspectives opened by these two methods but also their inherent limits explain that there is space for an alternative approach. The importance of working at low relative xenon concentration is obvious: it is the only way to ensure firstly that only specific interactions are detected, leading to a cartography of the hydrophobic regions; secondly that the pressure effect is not sufficient to give rise to a distortion of the protein. Thirdly, the formation of xenon clathrates due to the presence of a consequent amount of dissolved gas is avoided [18]. Up until now xenon NMR has been widely used to detect hydrophobic regions in biomolecules, but mainly indirectly. Tilton and Kuntz were pioneers in this field, with their study of the ^{129}Xe chemical shift in metmyoglobin [19]. The upfield shifts with increasing metmyoglobin concentration were attributed to the predominant influence of specifically bound xenon species to the overall shift. However, non-specific interactions between xenon and the external surface of myoglobin were shown through a comparison of the ^{129}Xe chemical shifts and longitudinal relaxation times for the protein denatured and under native conditions [20]. Similar results were obtained for other proteins such as mutants of Lyzozyme T4 [10], maltose binding protein [21] or other lyophilized proteins [22]. Xenon is indeed able to explore a large number of interaction sites at the surface of the protein, and the variation of the observed chemical shift becomes representative of specific and non-specific interactions [23].

However, in order to locate xenon atoms relative to the protein nuclei, the recourse to dipole–dipole cross-relaxation becomes mandatory. In 1996 Pines and co-workers have proposed, under the acronym SPINOE 'Spin Polarization Induced NOE' [24], an approach designed to demonstrate such through-space interaction from laser-polarized xenon to other nuclei. It had been applied not only for the detection of xenon-solvent [24] or xenon-surface interactions [25], but also for the study of the xenon binding in cage-molecules in organic solvents [26,27]. Having developed a SPINOE pulse sequence of high stability, we extended these experiments in water, where the lower solubility of xenon requires a higher xenon magnetization. The study of α-cyclodextrin in

D_2O revealed the through-space interaction of xenon with mainly two proton signals of the host: the protons H-3 and H-5 located at the interior of the rim, confirming that this approach could represent a way to cartography hydrophobic cavities [28]. We had extended this approach by characterizing an hydrophobic cavity of a protein, the wheat non-specific Lipid Transfer Protein [11,29]. This experiment proved that, at ambient pressure, it was feasible to probe hydrophobic regions of biomolecules thanks to selective polarization transfer from dissolved laser-polarized xenon. In the following sections, we focus on the description of the principles of this selective polarization transfer, discussing the difficulties and solutions developed to overcome them.

3. Location of xenon in hydrophobic regions via polarization transfer

3.1. Principle of the selective SPINOE experiment

Laser-polarized xenon can be seen as a system at very low spin temperature [30]. For instance, in a field of 14 T a xenon sample polarized at 20% corresponds to a spin temperature of 20 mK. Being at such low temperature, it induces a cool down of the spin systems in contact, such as the protons of the solvent, which, due to cross-relaxation, experience a change of their spin temperature, i.e., a change of their net polarization. The principle of the SPINOE approach is to monitor this variation [24]. In their initial proposition, Pines and coworkers directly observed the temporal evolution of the intensities of the solvent peak by acquiring NMR spectra after low flip angle. The observed proton signal enhancement has risen a hope for using laser-polarized xenon as a source of nuclear polarization. It remains that, as shown below, this enhancement is strongly dependent on the relative magnetization of the xenon and proton nuclei, on the xenon–proton cross-relaxation rate σ_{XeH} and on the proton longitudinal self-relaxation time.

Often, the situation is not as simple as in deuterated benzene, because of the presence of different protons H_i efficiently coupled together by dipolar cross-relaxation. Noting I_z^i and S_z the proton and xenon magnetization, the spin dynamics can be described by the following set of generalized Solomon equations:

$$\frac{\mathrm{d}I_z^i}{\mathrm{d}t} = -\rho_{\mathrm{H}^i}\left(I_z^i - I_0\right) - \sum_{j\neq i}\sigma_{\mathrm{H}^i\mathrm{H}^j}\left(I_z^j - I_0\right) - \sigma_{\mathrm{XeH}^i}(S_z - S_0), \tag{1}$$

$$\frac{\mathrm{d}S_z}{\mathrm{d}t} = -\rho_{\mathrm{Xe}}(S_z - S_0) - \sum_{i}\sigma_{\mathrm{XeH}^i}\left(I_z^i - I_0\right), \tag{2}$$

where ρ_{H^i}, ρ_{Xe} are the proton and xenon self-relaxation rates, $\sigma_{\mathrm{H}^i\mathrm{H}^j}$ the homonuclear dipolar cross-relaxation rates and I_0 and S_0 the proton and xenon thermal equilibrium polarizations. In the following we shall neglect S_0 relative to S_z. The integration of the system of differential equations reveals that the proton magnetization I_z^i at time t depends on the xenon magnetization and the xenon–proton cross-relaxation but also of the proton thermal equilibrium value, of the initial proton magnetization (initial conditions) and of the full proton relaxation matrix. In the present paper in order to locate the noble gas, we are interested in the observation and quantification of selective magnetization transfer from dissolved laser-polarized xenon to protons. Considering the low intermolecular heteronuclear cross-relaxation rates expected, the contribution from the direct proton magnetization I_0 has to be removed, the initial proton magnetization and the duration τ_m of the contact time between proton and xenon magnetization have to be known. This explains that selective SPINOE is usually implemented as a difference spectroscopy [26].

3.2. Approaching quantification: control of the proton–proton cross-relaxation

The big diameter of the xenon atom, its gyromagnetic ratio about 4 times lower than that of the proton, the low occupancy factor usually encountered when bound into hydrophobic cavities and the small xenon–proton correlation times reported so far [31] imply that the xenon–proton cross-relaxation rates are several orders of magnitude lower than the intramolecular proton–proton cross-relaxation rates. Due to this, as soon as the xenon polarization is transferred to the nearby protons of the protein through dipole–dipole interaction, it is 'diluted' to the more remote protons. To quench this spin-diffusion, several solutions are possible, but the one presenting the least drawbacks consists in using a proton off-resonance rf field during the mixing period. The efficiency of this approach, called SPIROE, has been experimentally demonstrated on a cage-molecule, cryptophane-233 in tetrachloroethane [32]. By an adequate choice of the strength of this field and/or its frequency offset, it is possible to make the proton–proton cross-relaxation vanish. These choices define an angle θ_{H} between the static and effective field axes experienced by the nuclei. The characteristic relaxation rates of the SPIROE can be expressed as a function of the longitudinal ($\theta_{\mathrm{H}} = 0°$) and transverse ($\theta_{\mathrm{H}} = 90°$) rates [32,33]:

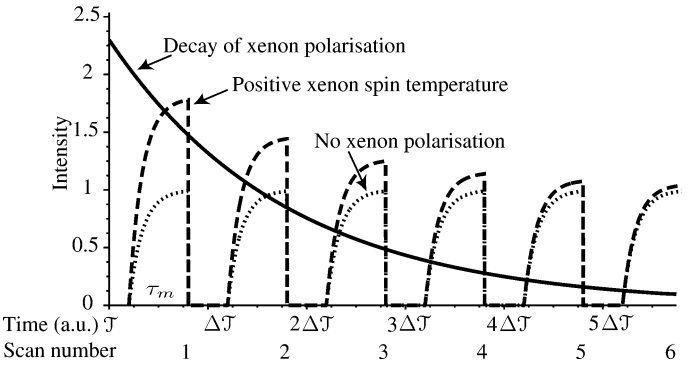

Fig. 1. Schematic description of the evolution of xenon and proton magnetization during SPIROE experiment, taking into account the transient character of the laser-polarized xenon spin temperature. It is assumed that the proton spin-diffusion is quenched. Solid line: xenon polarization decay. Dashed and dotted lines: evolution of the proton magnetization in successive SPIROE experiments. The first part of each SPIROE experiment is the proton saturation, the second is the mixing time τ_m during which proton magnetization buildup occurs. Dashed line: laser-polarized xenon with positive spin temperature, dotted line: no xenon polarization. The selective SPIROE experiment usually consists in measuring the difference between the dashed and the dotted lines. The relative xenon and proton ordinate scaling is not respected. In realistic experimental conditions, the decay of xenon magnetization is typically tuned to be about 20 times slower than in this schematic representation.

$$\rho_{\mathrm{H}}^{\theta_{\mathrm{H}}} = \rho_{\mathrm{H}}^{0^\circ} \cos^2\theta_{\mathrm{H}} + \rho_{\mathrm{H}}^{90^\circ} \sin^2\theta_{\mathrm{H}}, \tag{3}$$

$$\sigma_{\mathrm{XeH}}^{\theta_{\mathrm{H}}} = \sigma_{\mathrm{XeH}}^{0^\circ} \cos\theta_{\mathrm{H}}. \tag{4}$$

Finally, the steady state value of the proton magnetization becomes dependent on the angle θ_{H} [33,34]. In these conditions, the Solomon equations become:

$$\frac{\mathrm{d}I_z}{\mathrm{d}t} = -\rho_{\mathrm{H}}^{\theta_{\mathrm{H}}}\left(I_z - I_0^{\theta_{\mathrm{H}}}\right) - \sigma_{\mathrm{XeH}}^{\theta_{\mathrm{H}}} S_z, \tag{5}$$

$$\frac{\mathrm{d}S_z}{\mathrm{d}t} = -\rho_{\mathrm{Xe}} S_z - \sigma_{\mathrm{XeH}}^{\theta_{\mathrm{H}}}\left(I_z - I_0^{\theta_{\mathrm{H}}}\right). \tag{6}$$

Essentially in a selective SPIROE experiment, the xenon magnetization evolves slowly relative to the proton magnetization ($\rho_{\mathrm{Xe}} \ll \rho_{\mathrm{H}}^{\theta_{\mathrm{H}}}$). We can integrate Eq. (5) with the initial condition due to proton magnetization saturation $I_z(\mathcal{T}, 0) = 0$. At any moment $\mathcal{T}$, each buildup curve of Fig. 1 is then described by:

$$I_z(\mathcal{T}, \tau_m) = \left(I_0^{\theta_{\mathrm{H}}} - \frac{\sigma_{\mathrm{XeH}}^{\theta_{\mathrm{H}}}}{\rho_{\mathrm{H}}^{\theta_{\mathrm{H}}}} S_z(\mathcal{T})\right)\left(1 - \exp\left(-\rho_{\mathrm{H}}^{\theta_{\mathrm{H}}}\tau_m\right)\right). \tag{7}$$

We can define the selective proton magnetization enhancement $\Delta I(\mathcal{T}, \tau_m)$ for a mixing time τ_m as the difference between the proton magnetization in the presence of xenon magnetization $S_z(\mathcal{T})$ and in its absence $S_z(\infty) = 0$:

$$\Delta I(\mathcal{T}, \tau_m) = I_z(\mathcal{T}, \tau_m) - I_z(\infty, \tau_m) = -\frac{\sigma_{\mathrm{XeH}}^{\theta_{\mathrm{H}}}}{\rho_{\mathrm{H}}^{\theta_{\mathrm{H}}}} S_z(\mathcal{T})\left(1 - \exp\left(-\rho_{\mathrm{H}}^{\theta_{\mathrm{H}}}\tau_m\right)\right). \tag{8}$$

Four remarks result from this equation:

- the sign of the variation of the proton magnetization is defined by the sign of the laser-polarized xenon spin temperature;
- the proton magnetization enhancement $\Delta I(\mathcal{T}, \tau_m)$ is proportional to the xenon magnetization $S_z(\mathcal{T})$. The signal enhancement consequently decreases when the xenon magnetization relaxes, as is clearly observable in Fig. 1;
- the maximal enhancement is proportional to the ratio of the heteronuclear cross–relaxation rate to the proton self-relaxation rate. However, the biggest variation deals with the proton self-relaxation, which explains the very peculiar case of partially deuterated benzene ($1/\rho_{\mathrm{H}}^{0^\circ} \simeq 160$ s), and could explain the fact that methyl-rich regions are exhausted in SPINOE experiments on proteins [11];
- the proton buildup rate during the mixing time is defined by the proton self-relaxation and not by the heteronuclear cross-relaxation $\sigma_{\mathrm{XeH}}^{\theta_{\mathrm{H}}}$ even if the initial slope of the difference $\mathrm{d}\Delta I(\mathcal{T}, \tau_m)/\mathrm{d}\tau_m$ is equal to $-\sigma_{\mathrm{XeH}}^{\theta_{\mathrm{H}}} S_z(\mathcal{T})$. This mainly means that the optimum τ_m value to observe SPIROE is defined by $\rho_{\mathrm{H}}^{\theta_{\mathrm{H}}}$ [32].

The combined study of Eqs. (3), (4) and (8) and the expression of the relaxation rates as a function of the spectral densities [33] lead to the three following remarks about the use of off-resonance rf irradiation. Firstly $\rho_{\mathrm{H}}^{\theta_{\mathrm{H}}} > \rho_{\mathrm{H}}^{0^\circ}$, so a shorter mixing time τ_m is needed. Secondly, the relative signal enhancement $\Delta I(\mathcal{T}, \tau_m)/I_z(\infty, \tau_m)$, which is relied to the capability of detecting the polarization transfer, is independent of θ_{H}. The net effects of the off-resonance rf irradiation of the proton are consequently a gain in quantification and in cycling delay, since shorter τ_m – and thus shorter $\Delta\mathcal{T}$ values – can be used.

3.3. Implementing the SPINOE experiment

The implementation of selective SPINOE should allow the detection of very low signal enhancements $\Delta I(\mathcal{T}, \tau_m)$, since they typically represent between 0.001 and 0.1 of the direct signal $I_z(\infty, \tau_m)$. Such signals can be measured by NMR but a very stable pulse sequence is required.

The selective SPINOE scheme requires knowledge of the proton spin state at the beginning of each mixing time. The trivial method consists in saturating the proton magnetization [26]. Among the different ways proposed and tested, a series of 90° pulses each followed by a pulsed field gradient of random amplitude seems the best solution to achieve this goal in the shortest time. Indeed, during this delay as well as during the acquisition of the proton NMR signal, one cannot take advantage for the proton signal enhancement of the presence of xenon magnetization since it relaxes. It is consequently of key importance to keep all delays, except the mixing time, as short as possible.

The selective SPINOE experiment corresponds to a difference spectroscopy between the proton NMR signal in contact with laser-polarized xenon $S_z(\mathcal{T})$ and in contact with thermal xenon $S_z(\infty)$. An alternative would be the comparison to the proton magnetization in contact with laser-polarized xenon of opposite spin temperature. The sense of the xenon polarization can be chosen during the optical pumping step through orientation of the quarterwave plate or the direction of the magnetic field. However, the need for a high stability sequence precludes this method: the level of xenon polarization being susceptible to vary between successive optical pumping stages, the delay before the start of the NMR experiment being not constant, etc. Two solutions for the selective SPINOE remain: (i) waiting for a time $\mathcal{T}$ long versus $T_{1\mathrm{Xe}}$, a solution which does not require a xenon channel on the NMR probehead or inverting the xenon magnetization; (ii) if the proton signal enhancement is obtained thanks to the difference between two proton spectra whose acquisition is separated by the duration $\Delta\mathcal{T}$ and with opposite xenon magnetization, the extracted signal enhancement is:

$$I_z(\mathcal{T}, \tau_m) - I_z(\mathcal{T} + \Delta\mathcal{T}, \tau_m) = -\frac{\sigma_{\mathrm{XeH}}^{\theta_{\mathrm{H}}}}{\rho_{\mathrm{H}}^{\theta_{\mathrm{H}}}}\big(S_z(\mathcal{T}) + S_z(\mathcal{T} + \Delta\mathcal{T})\big) \cdot \big(1 - \exp\big(-\rho_{\mathrm{H}}^{\theta_{\mathrm{H}}}\tau_m\big)\big) \tag{9}$$

$$= \Delta I(\mathcal{T}, \tau_m) + \Delta I(\mathcal{T} + \Delta\mathcal{T}, \tau_m). \tag{10}$$

It is consequently equal to the signal enhancement for the two acquisitions at $\mathcal{T}$ and $\mathcal{T} + \Delta\mathcal{T}$ compared to the thermal equilibrium value. The signal to noise ratio of the scheme with xenon inversion is $\sqrt{2}$ times higher than without xenon inversion. The real situation is however not so simple, since the relaxation of xenon decreases the proton magnetization enhancement (Eq. (8)) and then the signal to noise ratio does not evolve as the number of accumulations (Fig. 1). There is consequently an optimum value which depends on $\Delta\mathcal{T}$ and $T_{1\mathrm{Xe}}$. It can be computed, but for a 1D spectrum it is safer to determine it experimentally by storing all ^{1}H spectra and choosing its value during the processing.

When acquiring proton signals with inverted xenon magnetization every other scan seems the best choice in term of signal to noise ratio; however, the experimental situation is complicated by the difficulties encountered for efficiently inverting xenon magnetization. Indeed its strong magnetization can induce radiation dumping and non-linear effects. Experimentally we found efficient in the fast exchange case (fast at the xenon chemical shift time scale), i.e. in the case encountered for all proteins studied so far, to invert xenon magnetization thanks to a frequency sweep pulse of the CHIRP type combined with a pulsed field gradient [35]. The same sort of pulse was found to suffer from poor yield in the case of slow exchange observed for xenon in cryptophanes. Indeed, in these systems the binding constants are generally high and the xenon chemical shift differences between the peaks of xenon free in the solvent and bound xenon can take values of more than one hundred ppm, more due to the global shielding effect due to relative volume of the cavity and the xenon atom than to the ring current effects of the aromatic groups [36]. Actually, the bad inversion of xenon magnetization can easily strongly reduce the apparent xenon T_1 during a SPINOE experiment. The previous theoretical description shows that it can be restored by a clever choice, dependent on $\Delta\mathcal{T}$ and on $T_{1\mathrm{Xe}}$, of the order in which the spectra with positive and negative xenon spin temperatures are acquired.

4. The SPIROE-TOCSY experiment

4.1. Choice of the experimental conditions

The transient character of the xenon magnetization represents a major drawback, which for instance, led us to assign SPINOE signals for wheat nonspecific Lipid Transfer Protein only using 1D proton sub-spectra [11]. Resorting to a 2D experiment for the assignment of these protons would obviously help, but its implementation is not as simple. A prerequisite for 2D NMR is that the proton magnetization before the incremented delay be constant.

Let us consider a 2D experiment where the initial proton buildup takes place in the presence of off-resonance rf irradiation (SPIROE). For a system in exchange, the xenon self-relaxation rate:

$$\rho_{\mathrm{Xe}} = \frac{1}{T_{1\mathrm{Xe}}} = f\frac{1}{T_{1\mathrm{complex}}} + (1-f)\frac{1}{T_{1\mathrm{free}}} \tag{11}$$

is relied to the amount of host through the fraction of bound xenon f. The proton signal enhancement $\mathcal{S}(\mathcal{T})$ at time $\mathcal{T}$ is:

$$\mathcal{S}(\mathcal{T}) = f S_z(0)\frac{\sigma_{\mathrm{XeH}}^{\theta_{\mathrm{H}}}}{\rho_{\mathrm{H}}^{\theta_{\mathrm{H}}}}\left(1-\mathrm{e}^{-\rho_{\mathrm{H}}^{\theta_{\mathrm{H}}}\tau_m}\right)\mathrm{e}^{-\mathcal{T}/T_{1\mathrm{Xe}}}. \tag{12}$$

The first temporal term of Eq. (12) represents the proton magnetization buildup, the second term the self-relaxation of laser-polarized xenon, which tends to diminish the signal enhancement. $\mathcal{T}$ is equal to the number of scans (ns) times the duration of one scan $\Delta\mathcal{T}$. Lowering the solute concentration decreases the relaxation rate of xenon but at the price of a lower signal $\mathcal{S}(\mathcal{T})$. In order to maximize the 2D SPINOE signal, the mixing time τ_m and the ratio of xenon to solute concentrations should be optimized. Through a differentiation of $\mathcal{S}$ relative to f and τ_m, the following solutions are obtained:

$$\left(\frac{\partial\mathcal{S}}{\partial\tau_m}\right)_f = 0 \quad\Longrightarrow\quad \tau_m = \frac{1}{\rho_{\mathrm{H}}^{\theta_{\mathrm{H}}}}\ln\left(\frac{\rho_{\mathrm{H}}^{\theta_{\mathrm{H}}}T_{1\mathrm{Xe}}}{\mathrm{ns}}+1\right), \tag{13}$$

$$\left(\frac{\partial\mathcal{S}}{\partial f}\right)_{\tau_m} = 0 \quad\Longrightarrow\quad \frac{1}{f} = \mathcal{T}\left(\frac{1}{T_{1\mathrm{complex}}} - \frac{1}{T_{1\mathrm{free}}}\right). \tag{14}$$

As a consequence, the measurement of the relaxation time of bound xenon $T_{1\mathrm{complex}}$ [31] as well as the estimation of the proton self-relaxation rates through off-resonance ROESY experiments [33] enable the optimization of the SPIROE mixing time, of the concentration ratio and of the protocol.

The decay of the xenon magnetization along $\mathcal{T}$ induces a variation of the proton magnetization at the beginning of this evolution time, and thus a broadening of the signal after double Fourier transformation in the indirect dimension dependent on the variation of $S_z(\mathcal{T})$. Noting T_2^{app} the apparent proton decay time in the indirect dimension and T_2 the proton transverse self-relaxation time, one finds:

$$\frac{1}{T_2^{\mathrm{app}}} = \frac{1}{T_2} + \frac{\Delta\mathcal{T}}{T_{1\mathrm{Xe}}\,\mathrm{dw}_1} \tag{15}$$

with dw_1 the increment time in the indirect dimension. Numerical applications reveal a nonnegligible contribution of the xenon decay during the 2D experiment to the linewidth in the indirect dimension. The resolution is, however, mainly limited by the number of FIDs in this dimension. Moreover, the knowledge of the xenon relaxation time can allow one to compensate from this decay during the processing step, as for the FLASH method [37].

4.2. The 2D SPIROE-TOCSY pulse sequence

Among all pulse sequences used to assign proton resonances we have decided to focus on the TOCSY (Fig. 2). This choice benefits from several advantages. In its sensitivity improvement by gradients implementation [38], no phase cycling is required, a nice feature when the magnetization before the evolution time is not constant. The signal to noise ratio is multiplied by $\sqrt{2}$ relative to a conventional experiment. Also this pulse sequence gives pure in-phase cross- and direct-peaks. As a consequence, the analysis of the 2D SPIROE-TOCSY maps should allow the distinction of the protons in through-space interaction with xenon – the sign of their peaks is known according to the initial xenon spin temperature (Eq. (8)) – from artifacts resulting from bad subtraction or from temperature or homogeneity fluctuations during the 2D acquisition. We have decided to implement the sequence by acquiring firstly the full 2D map without perturbing the xenon magnetization and then the full 2D map with inverted xenon magnetization only during the mixing time [28]. By this choice we benefit from a longer apparent $T_{1\mathrm{Xe}}$ since the decay of xenon magnetization due to diffusion or imperfect inversion pulses is avoided.

4.3. Experimental illustration

For some cryptophanes in organic solvents, the binding constant is high and the close proximity of the included xenon atom and protons of the cavity make that significant SPINOE are observed [27,32]. Consequently they can serve as model systems for the development or optimization of SPINOE-type approaches. The strong response to polarization transfer from laser-polarized xenon (proton signal enhancement of few tens of percent) allows the reduction of the number of scans in the SPINOE sub-spectra, and let us envisage 2D experiments. The situation would be quite different for proteins, since the lower xenon solubility in water and the small binding constant encountered so far give rise to proton signal enhancements of only few percent.

As a demonstration, a 2D SPIROE-TOCSY experiment has been performed on a cryptophane derivative in deuterated 1,1,2,2 tetrachloroethane (Fig. 3). The goal of such an experiment is to determine according to their precession frequency in the indirect dimension which protons experience through-space interactions with xenon. The cross-peaks indicate the connectivity pathways between these protons and other protons through scalar coupling, facilitating the identification of the proton signals, firstly by the separation of the resonances in both dimensions, secondly by the recognition of the spin systems. Fig. 4 displays the contour plot of such an experiment applied on compound **1** ((+)cryptophane A (−)camphanate) [41]. On the diagonal, only the aromatic protons (signal enhancement $\Delta I/I \sim 0.6$) and some protons of the ethylene dioxide linkers ($\Delta I/I \sim 0.2$) appear in pure absorption. The methoxy proton signals appear in dispersive mode. The diagonal peaks in the insert correspond to the camphanic ester moiety and exhibit a dispersive character. The methylene bridges linking the cyclotriveratrylene groups give no or poor diagonal signals as in the 2D TOCSY experiment, but cross-peaks at their frequency in F1 show through-bond interactions. The lack of symmetry of the contour plot indicates that some magnetization transfers are privileged. For instance, after having fully assigned the proton signals of **1**, it is interesting to note that the line at $\omega_1 = 4.5$ ppm corresponds to the methylene proton pointing toward the center of the cyclotriveratrylene group (here denoted 'endo'). The cross-peak at this F1 frequency corresponds to the geminal proton ($\omega_2 = 3.3$ ppm). This indicates that the magnetization transfer is the following: from xenon to 'endo' protons, and then through-bond to 'exo' protons (i.e., pointing in the direction opposite to the cyclotriveratrylarene groups). In contrast at $\omega_1 = 3.3$ ppm the weak signals detected are mainly in dispersive mode.

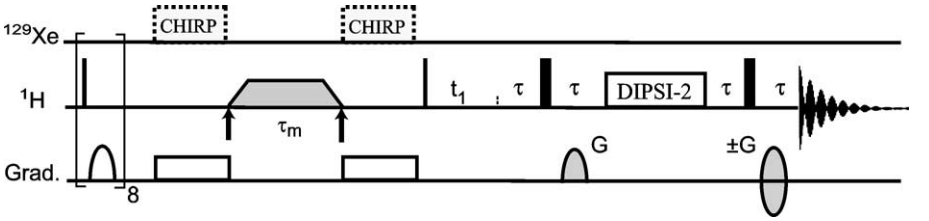

Fig. 2. SPIROE-TOCSY pulse sequence. The first part corresponds to the SPIROE experiment: it is composed of a saturation of the proton magnetization, followed during τ_m by the proton magnetization build-up in the presence of a proton off-resonance rf irradiation. The last part corresponds to the TOCSY. The narrow bars represent 90° hard pulses, the wide ones are 180° hard pulses. The gray trapezoid pulse corresponds to off-resonance rf irradiation (frequency switch at the position of the arrows) shaped in order to adiabatically rotate magnetization between the static and effective fields [39]. The multi-pulse sequence of the TOCSY is a DIPSI-2 [40]. The gray gradients corresponds to encoding ones [38]. This 2D experiment is run twice. For the first one, no adiabatic frequency sweep pulses (CHIRP) are applied on the xenon channel. On the second one they are present at the beginning and the end of the mixing time τ_m.

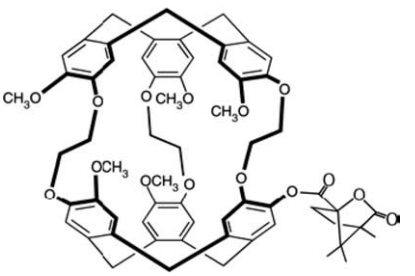

Fig. 3. Chemical structure of the (+)cryptophane A (−)camphanate compound **1**.

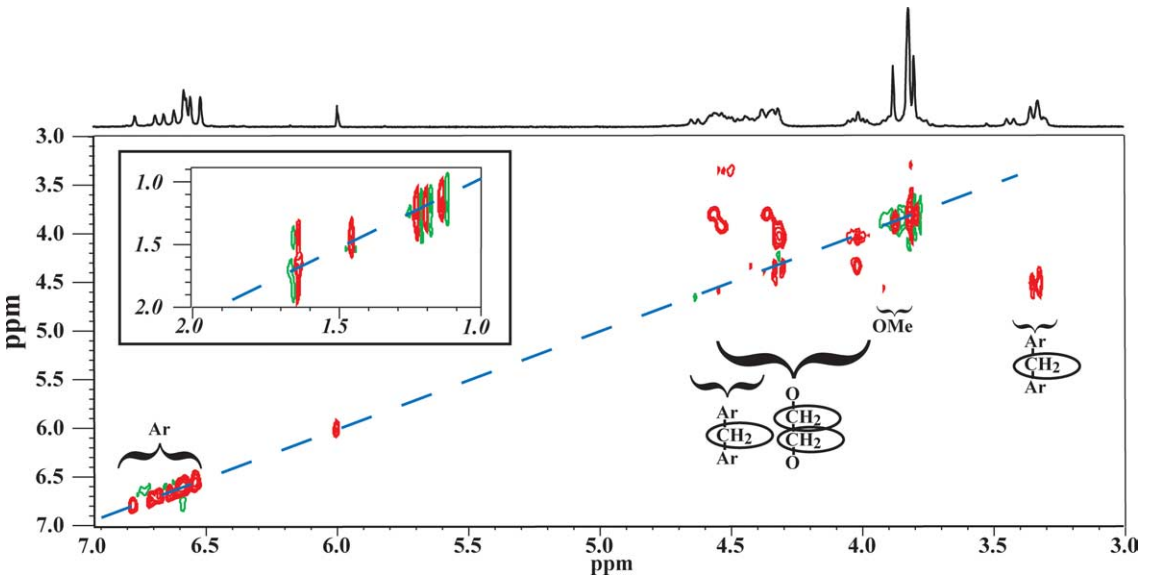

Fig. 4. 2D SPIROE-TOCSY performed on compound **1** in deuterated 1,1,2,2 tetrachloroethane. Experimental conditions: $T = 270$ K; magnetic field 11.7 T; inverse broadband probehead; concentration of **1** = 0.9 mM; pressure in the NMR tube: 0.9 atm, i.e. $f \sim 0.01$. 96% enriched xenon in isotope 129 is used. It is polarized with negative spin temperature to about 25% using the experimental apparatus described in [28]. SPIROE mixing time: 290 ms as optimized experimentally; $\theta_H = 32°$ as experimentally determined by off-resonance ROESY experiments [39]; rf field strength: 8.3 kHz; TOCSY spin-lock time: 25 ms; 4 scans per t_1 value; each 2D map is composed of 64 FIDs. The total experiment time is 4.5 minutes. The dashed line indicates the diagonal. The insert shows the region of the camphanic ester protons. Red contours correspond to positive peaks, green contours to negative peaks.

5. Perspectives

Since the description of polarization transfer from laser polarized xenon to solvent proton eight years ago, aiming at improving the NMR signal, many steps have already been made to extend this approach, in particular towards the mapping of hydrophobic protein cavities at ambient pressure and temperature. Different technical and theoretical improvements have allowed access to the quantification of the polarization transfer, to the estimation of the xenon dynamics inside cavities and, with the present paper, to an easier assignment of the SPINOE peaks through two dimensional NMR. This progress, in association with technical steps designed to increase the amount of highly polarized xenon produced and its efficient release to the sample, may open the way to the development of an efficient strategy for mapping all surface regions of a protein with hydrophobic properties and their behavior during molecular recognition.

Acknowledgements

HD and PB would like to take benefit of this paper to acknowledge Professor Maurice Goldman, not only for having introduced them to relaxation theory, in particular in the presence of off-resonance rf irradiations more than twelve years ago, but to still be their privileged interlocutor on many subjects. We greatly acknowledge Drs. T. Brotin and J.P. Dutasta from École Normale Supérieure de Lyon for providing us cryptophane **1**. The French Research Ministry is acknowledged for financial support (ACI #4103).

References

[1] A. Kastler, J. Phys. Radium 11 (1950) 225.
[2] M.A. Bouchiat, T.R. Carver, C.M. Varnum, Phys. Rev. Lett. 5 (1960) 373–375.
[3] T.G. Walker, W. Happer, Rev. Mod. Phys. 69 (1997) 629–642.
[4] L. Darasse, G. Guillot, P.J. Nacher, G. Tastevin, C. R. Acad. Sci. Paris, Ser. IIb 324 (1997) 691–700.
[5] A. Bifone, Y.-Q. Song, R. Seydoux, R.E. Taylor, B.M. Goodson, T. Pietraß, T.F. Budinger, G. Navon, A. Pines, Proc. Natl. Acad. Sci. USA 93 (1996) 12932–12936.

[6] B.F. Chmelka, D. Raftery, A.V. McCormick, L.C. de Menorval, R.D. Levine, A. Pines, Phys. Rev. Lett. 66 (1991) 580–583.
[7] J.-L. Bonardet, J. Fraissard, A. Gédéon, M.-A. Springuel-Huet, Catal. Rev. Sci. Eng. 41 (1999) 115–225.
[8] T. Pietraß, J.M. Kneller, R.A. Assink, M.T. Anderson, J. Phys. Chem. B 103 (1999) 8837–8841.
[9] V.V. Terskikh, I.L. Moudrakovski, S.R. Breeze, S. Lang, C.I. Ratcliffe, J.A. Ripmeester, A. Sayari, Langmuir 18 (2002) 5653–5656.
[10] S.M. Rubin, S.-Y. Lee, E.J. Ruiz, A. Pines, D.E. Wemmer, J. Mol. Biol. 322 (2002) 425–440.
[11] C. Landon, P. Berthault, F. Vovelle, H. Desvaux, Protein Sci. 10 (2001) 762–770.
[12] B.W. Matthews, A.G. Morton, F.W. Dahlquist, Science 270 (1995) 1847–1848.
[13] J.A. Ernst, R.T. Clubb, H.X. Zhou, A.M. Gronenborn, G.M. Clore, Science 270 (1995) 1848–1849.
[14] R.F. Tilton, I.D. Kuntz, G.A. Petsko, Biochemistry 23 (1984) 2849–2857.
[15] T. Prangé, M. Schiltz, L. Pernot, N. Colloc'h, S. Longhi, W. Bourguet, R. Fourme, Prot. Struct. Funct. Gen. 30 (1998) 61–73.
[16] M.L. Quillin, W.A. Breyer, I.J. Grisworld, B.W. Matthews, J. Mol. Biol. 302 (2000) 955–977.
[17] G. Otting, E. Liepinsh, B. Halle, U. Frey, Nat. Struct. Biol. 4 (1997) 396–404.
[18] M. Schiltz, T. Prangé, R. Fourme, J. Appl. Crystallogr. 27 (1994) 950–960.
[19] R.F. Tilton, I.D.J. Kuntz, Biochemistry 21 (1982) 6850–6857.
[20] S.M. Rubin, M.M. Spence, B.M. Goodson, D.E. Wemmer, A. Pines, Proc. Natl. Acad. Sci. USA 97 (2000) 9472–9475.
[21] S.M. Rubin, M.M. Spence, I.E. Dimitrov, E.J. Ruiz, A. Pines, D.E. Wemmer, J. Am. Chem. Soc. 123 (2001) 8616–8617.
[22] C.R. Bowers, V. Storhaug, C.E. Webster, J. Bharatam, A. Cottone III, R. Gianna, K. Betsey, B.J. Gaffney, J. Am. Chem. Soc. 121 (1999) 9370–9377.
[23] E. Locci, Y. Dehouck, M. Casu, G. Saba, A. Lai, M. Lühmer, J. Reisse, K. Bartik, J. Magn. Reson. 150 (2001) 1–8.
[24] G. Navon, Y.-Q. Song, T. Rõõm, S. Appelt, R.E. Taylor, A. Pines, Science 271 (1996) 1848–1851.
[25] E. Brunner, R. Seydoux, M. Haake, A. Pines, J.A. Reimer, J. Magn. Reson. 130 (1998) 145–148.
[26] Y.-Q. Song, B.M. Goodson, R.E. Taylor, D.D. Laws, G. Navon, A. Pines, Angew. Chem. 36 (1997) 2368–2370.
[27] M. Lühmer, B.M. Goodson, Y.-Q. Song, D.D. Laws, L. Kaiser, M.C. Cyrier, A. Pines, J. Am. Chem. Soc. 121 (1999) 3502–3512.
[28] H. Desvaux, T. Gautier, G. Le Goff, M. Pétro, P. Berthault, Eur. Phys. J. D 12 (2000) 289–296.
[29] P. Berthault, C. Landon, F. Vovelle, H. Desvaux, C. R. Acad. Sci. Sér. IV 2 (2001) 327–332.
[30] M. Goldman, Spin Temperature and Nuclear Magnetic Resonance in Solids, Oxford University Press, Oxford, 1971.
[31] L. Dubois, S. Parrès, J.G. Huber, P. Berthault, H. Desvaux, J. Phys. Chem. B 108 (2004) 767–773.
[32] H. Desvaux, J.G. Huber, T. Brotin, J.-P. Dutasta, P. Berthault, ChemPhysChem 4 (2003) 384–387.
[33] H. Desvaux, P. Berthault, Prog. NMR Spectrosc. 35 (1999) 295–340.
[34] H. Desvaux, M. Goldman, Mol. Phys. 81 (1994) 955–975.
[35] P. Berthault, H. Desvaux, G. Le Goff, M. Pétro, Chem. Phys. Lett. 314 (1999) 52–56.
[36] D.N. Sears, C.J. Jameson, J. Chem. Phys. 119 (2003) 12231–12244.
[37] A. Haase, J. Frahm, D. Matthaei, W. Hänicke, K.-D. Merboldt, 67 (1986) 258–266.
[38] J. Cavanagh, M. Rance, Ann. Rep. NMR Spectroscopy 27 (1993) 1–58.
[39] H. Desvaux, P. Berthault, N. Birlirakis, M. Goldman, J. Magn. Reson. A 113 (1995) 47–52.
[40] A.J. Shaka, C.J. Lee, A. Pines, J. Magn. Reson. 77 (1988) 274–293.
[41] T. Brotin, R. Barbe, M. Darzac, J.P. Dutasta, Chem. Eur. J. 9 (2003) 5784–5792.